Photoproduction of Positive Pions in Hydrogen in the Angular Range $7° < \theta_{c.m.} < 27°$ and Photon Energy Range 220 Mev $< k <$ 390 Mev*†

ALAN J. LAZARUS,‡ W. K. H. PANOFSKY, AND F. R. TANGHERLINI,§
Department of Physics and High-Energy Physics Laboratory, Stanford University, Stanford, California
(Received October 20, 1958)

Relative measurements of the cross sections for the production of positive pions by photons on protons have been carried out in the range of c.m. angles $7° < \theta_{c.m.} < 27°$ for four photon energies from 220 to 390 Mev. Positive pions were detected via the decay positron from the $\pi-\mu-e$ chain which was observed in a series of gates following a pulse of photons and electrons from the Mark III linear accelerator. The results have been compared with new dispersion theory calculations using a range of values of the coupling constant and resonance energy. The experimental data at these small angles are in good agreement with the calculations; however, the fit of the calculations with available data at larger angles is not satisfactory. It is shown that the fit in either case is substantially poorer if the so-called "retardation term," i.e., the diagram in which the photon is absorbed by a virtual meson, is omitted.

I. INTRODUCTION

THE angular distribution of photopions at small angles has recently been the subject of considerable experimental interest.[1–4] The motivation for these measurements has been principally the investigation of the so-called "retardation term": that particular diagram in which the incident photon is absorbed on a pion virtually emitted by the proton. This term differs from the remaining terms in photoproduction (in which the photon is absorbed by an electromagnetic interaction with the nucleon followed by a pion rescattering on the nucleon) in that the electromagnetic interaction permits all spherical harmonics to be present in the amplitude of the retardation term. The final state interaction involved in the remaining terms causes the order of spherical harmonics to be limited by the momentum of the pion and the range of the pion-nucleon interaction.

The amplitude of the retardation term is of the form $\sin\theta/(1-\beta\cos\theta)$, where β is the pion velocity. The denominator represents the retarded interaction of the pion and the electromagnetic field and results in the amplitude's becoming a maximum at small angles.

The theoretical expression for the retardation term corresponds to an essentially classical photoelectric result and is insensitive to our information on the meson-nucleon interaction. The possibility of separating it from the other terms in the pion photoproduction matrix element is unfortunately impaired by uncertainties in these other terms and in particular by the relatively poor fit of the experimental data on π^+ production and dispersion-theoretical calculations.

There are two possible approaches to "establishing" the existence of the retardation term: the first is to fit the calculations of Chew *et al.*[5] with and without the term in question; the second[4] is to show that a fit to the angular distribution of the form $A+B\cos\theta+C\cos^2\theta$ is incompatible with the observed angular distribution.

In Fig. 1 we show curves computed with and without the retardation term from the calculations of Chew *et al.*[5]; details are given in Sec. V. Note that the retardation term contributes very significantly at large angles as well. Below resonance, the influence of the term is reduced by interference with other contributions. Because of this fact and of the uncertainties of the calculations, the data reported here are not a

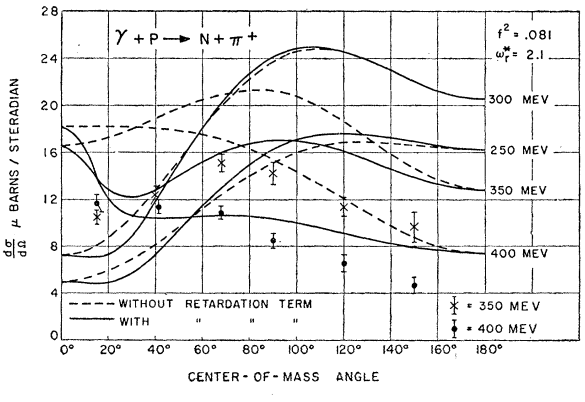

FIG. 1. Plot of the experimental photoproduction data of Walker *et al.* (see reference 12) at 350 and 400 Mev *vs* c.m. angle. Shown are curves computed from the dispersion relations of Chew *et al.* (see reference 5) (solid lines) by methods discussed in Sec. V; also shown are the same computations with the retardation term omitted.

* Supported by the joint program of the Office of Naval Research, the U. S. Atomic Energy Commission, and the Air Force Office of Scientific Research.

† A more detailed version has been submitted by A. J. Lazarus as a doctoral dissertation to Stanford University.

‡ Now at RAND Corporation, Santa Monica, California.

§ Now at the Institute for Theoretical Physics, Copenhagen, Denmark.

[1] Richter, Osborne, and Russell, *Proceedings of the CERN Symposium on High-Energy Accelerators and Pion Physics, Geneva, 1956* (European Organization of Nuclear Research, Geneva, 1956), Vol. 2, p. 284; and B. Richter (private communication).

[2] Perez-Mendez, Imhoff, Kenney, and Knapp (private communication); and E. A. Knapp, University of California Radiation Laboratory Report UCRL-8354, 1958 (unpublished).

[3] R. D. Miller and R. M. Littauer (private communication).

[4] J. H. Malmberg and C. S. Robinson, Phys. Rev. **109**, 158 (1958).

[5] Chew, Goldberg, Low, and Nambu, Phys. Rev. **106**, 1345 (1957).

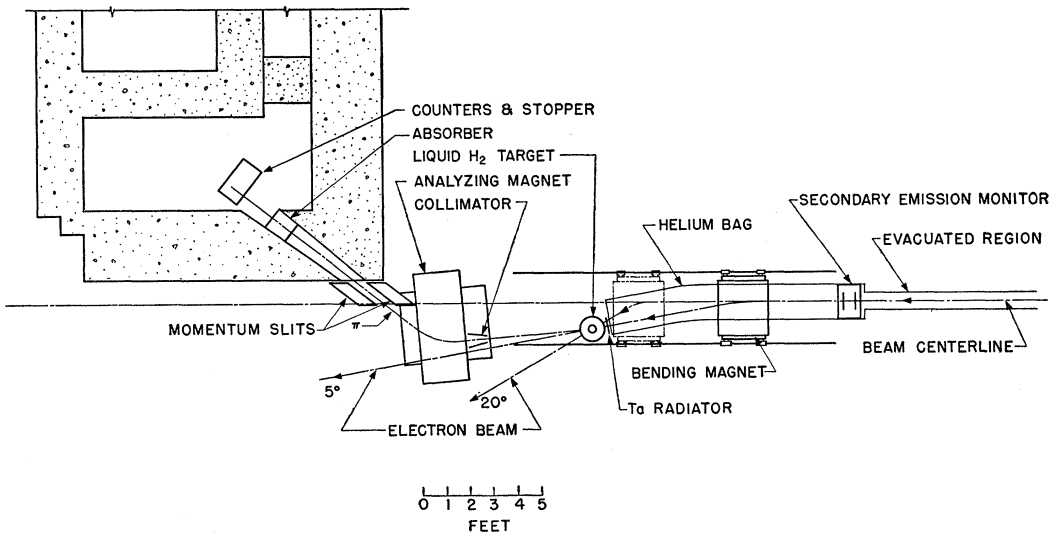

FIG. 2. Diagram of the experimental arrangement. Note that the entire detecting arrangement—consisting of collimator, analyzing magnet, absorbers, stopper and counter—is stationary, while the incident electron beam can be deflected, thus changing the pion production angle.

test of specific features of the theory, but simply extend the available data at small angles to higher energy.

II. EXPERIMENTAL APPARATUS

Principle of Detection

The experimental arrangement is shown in Fig. 2. The energy-analyzed electron beam from the Mark III linear accelerator is bent by a magnet and passes through a 0.020-in. tantalum radiator and a liquid-hydrogen target. Pions produced in the target which pass through a collimator are momentum-analyzed and enter a channel leading to the counters. The pions are slowed by a carbon absorber whose thickness was chosen so that pions passed by the analyzing magnet will stop in another block of carbon called the "stopper."

The presence of a stopped pion is indicated by observing the positron from the $\pi^+ - \mu^+ - e^+$ decay chain through a series of gates timed at suitable intervals after the beam pulse.

Electron Beam

The electron beam arrives at the experimental area after it has been magnetically-analyzed in order to define its momentum and momentum width. The central momentum defined by the analyzing system has been calibrated by W. M. Woodward to an accuracy of $\pm 0.5\%$. To obtain maximum beam current, the momentum-selecting slits in the beam-analyzing apparatus were set at a 2% total width, which is about equal to the momentum spread of the principal part of the unanalyzed electron beam. A beam pulse of 0.1-μsec length was used.

Beam Monitoring

The incident beam was monitored by integrating the secondary emission current from a series of alternately biased 0.001-in. aluminum foils traversed by the electron beam.[6] A measurement of the energy dependence of this system of beam monitoring, accomplished by comparing its results with those of a Faraday cup, showed a change of less than 0.3% in efficiency from 0 to 300 Mev.[7] Two recent comparisons of the monitor efficiency with a Faraday cup in the range of this experiment disagreed slightly: one showed no change in efficiency and the other a 4% increase in efficiency over the energy range covered. This uncertainty in monitoring efficiency is included in the summary of errors discussed below.

Angle Determination

The angle made by the deflected beam and the axis of the collimator can be changed by moving the beam-bending magnet parallel to the original direction of the beam and varying the magnet current so that the deflected beam passes through the target (see Fig. 2). This technique was used in a previous experiment[8] on the electromagnetic pair production of μ mesons. The uncertainty of the angle measurement is less than 0.5° at 20° and decreases at smaller angles. The width of the collimator leading to the analyzing magnet, combined with the width of the target, introduces an angular width of $\pm 1°$.

[6] H. R. Fechter and G. W. Tautfest, Rev. Sci. Instr. **26**, 229 (1951).
[7] K. L. Brown and G. W. Tautfest, Rev. Sci. Instr. **27**, 696 (1956).
[8] G. E. Masek and W. K. H. Panofsky, Phys. Rev. **101**, 1094 (1956).

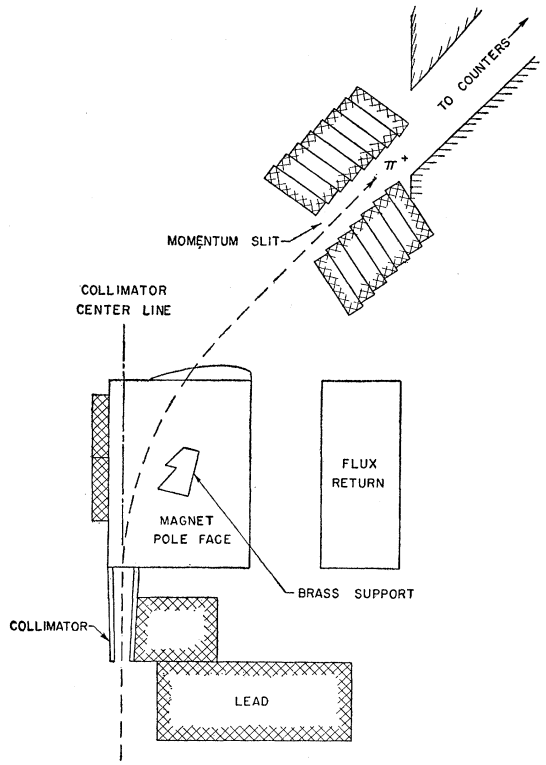

FIG. 3. Configuration of collimators and slits in the analyzing magnet.

Radiator

The radiator used in the experiment was 0.020-in. tantalum, which is equivalent to 0.11 radiation length if a thick-target correction is made to the thin-target Bethe-Heitler formula. The thickness is limited by the background due to the multiply-scattered electron beam's hitting the meson magnet and collimator in the 5° geometry. Because of space limitations, the electron beam was not swept out after the photons were produced. The background is still low at 7.5° but rises to approximately half the signal at 5°.

Target

The liquid hydrogen is held in a vacuum-jacketed, $3\frac{1}{2}$-in. diameter, aluminum cup whose walls form a vertical cylinder. The diameter allows a $\frac{1}{4}$-in. displacement of the beam parallel to a diameter with only a 1% change in hydrogen thickness traversed by the beam. The target is emptied for background runs by letting down the vacuum with helium and allowing the hydrogen to boil off.

Analyzing Magnet and Collimator

A magnet of standard design was re-assembled as a *C* magnet to avoid having the electron beam hit the magnet yoke. The entrance collimator was constructed of brass blocks which were aligned so that pions leaving the target could not scatter from their faces. The momentum range passed by the analyzing system was limited by the momentum slits following the analyzing magnet. The beam path is shown in Fig. 3.

The momentum selected by the magnet and slits was matched by choosing the thickness of the absorber. The choice was checked by running a curve of counting rate *vs* analyzing magnet current. A typical curve of the results is shown in Fig. 4. The tail of the curve seemed to indicate a sensitivity to particles of higher momenta. Checks carried out by calibrating the channel with elastically scattered electrons failed to confirm this tail on the resolution curve, and we conclude that it does not exist under conditions of constant magnet current. To check this point further, we observed the excitation curve of the production of positive pions detected by the apparatus at constant magnet current setting, and changing the photon spectrum by varying the primary beam energy. The theoretical and experimental points are shown in Fig. 5. Within the statistics of the experiment, the points are compatible with the points calculated assuming the acceptance indicated by the electron-scattering measurements.

Counters

Two scintillation telescopes, consisting of two members each, one above and one below the carbon stopper, were used to detect the positrons from the $\pi^+-\mu^+-e^+$ decay chain. The counters nearest the

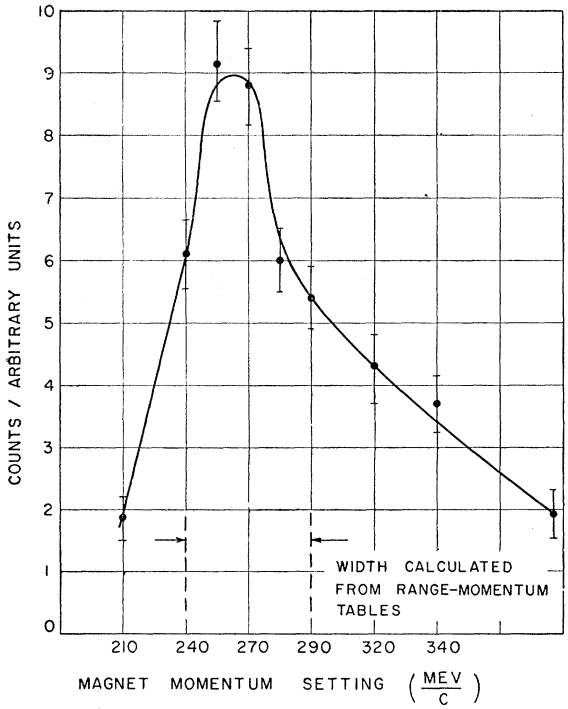

FIG. 4. Typical curve of pion counting rate *vs* magnetic field setting for fixed absorber.

stopper were pulsed off during the beam, to prevent overloading by prompt signals, by a disabling circuit described elsewhere.[8]

III. EXPERIMENTAL PROCEDURES AND DATA HANDLING

Data Schedule

Measurements were taken in the angular range $5° < \theta < 20°$ in 2.5° intervals in laboratory angle; data were taken at constant pion momentum. The momentum setting and corresponding absorbers were chosen to correspond to photon energies of 220, 300, 350, and 390 Mev.

The measurements were not absolute; "reference runs" taken at 3% statistics with a thicker radiator on positive pions of 60-Mev energy, were inserted in the data

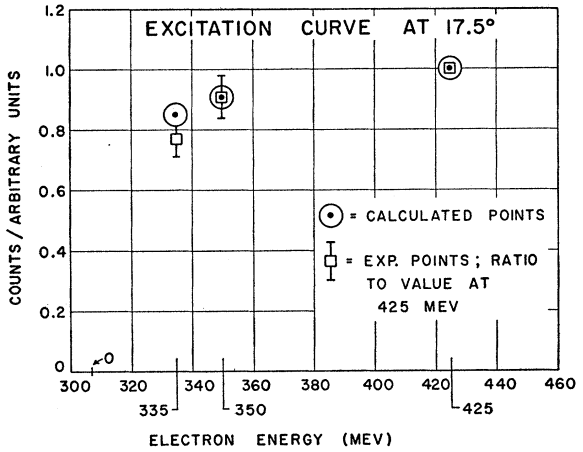

FIG. 5. Excitation curve of pion count observed at a fixed detector setting as a function of the incident electron energy. Shown are the experimental measurements (squares); and theoretical points computed taking into account (i) the Bethe-Heitler spectrum, (ii) thick-target bremsstrahlung calculations, (iii) the geometrical resolution of the analyzer, and (iv) the energy variation of the part of the pion yield produced directly by electrons.

runs. Backgrounds were taken by emptying the hydrogen target. Considering the thickness of the radiator (0.11 radiation length effective), and the small thickness of the target (0.011 radiation length), we assume that the background is not substantially affected by the presence of the liquid hydrogen. Figure 6 shows a typical set of background runs.

Angular Distribution Data

The accuracy of the data obtained here is considerably superior in regard to the angular distribution than in regard to the energy dependence of the cross sections. For this reason we shall discuss the data-handling procedures for these two purposes separately.

Using elastic electron scattering in carbon we carried out runs to explore the variation in geometrical acceptance of the magnet system with the position of the

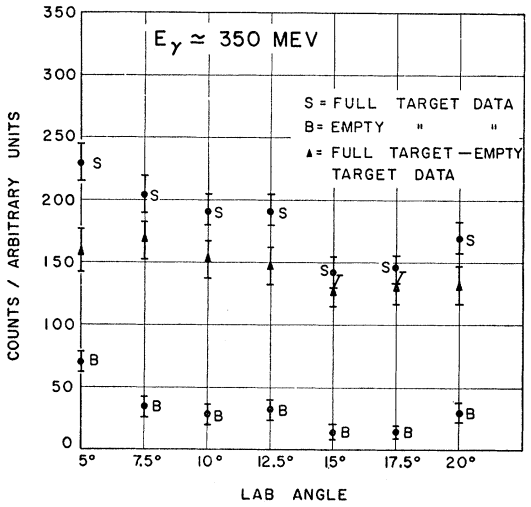

FIG. 6. Plot of the raw data at a pion analyzer setting corresponding to a photon energy of 350 Mev. Shown as a function of laboratory angle are counts with the liquid hydrogen target full, counts with the liquid hydrogen target empty, and the subtracted count (triangles).

scattering source point along the line of pion sources in hydrogen in the actual experiment. These runs showed the solid angle times the momentum band accepted to be independent of angle to better than 3%. Also, the angular resolution is constant to 1% over the range of angles. These conclusions were also reached by a graphical analysis of charged particle orbits.

Table I shows the angular distribution data at each energy. These data are proportional to the differential cross section in the c.m. system at each energy; the appropriate factors for the lab-c.m. solid angle transformation and the photon spectrum have been applied. Errors shown are statistical; the possible systematic errors discussed above are negligible.

Data on Energy Dependence of the Cross Section

To reduce the primary data in terms of the energy dependence of the cross section, numerous corrections have to be applied; some of these can be made with only limited accuracy. The situation is shown in Table II; section (a) contains the energy dependence of the various correction factors relative to the measurements at a photon energy $k = 220$ Mev; section (b) gives the corresponding uncertainties. We shall now discuss these corrections:

TABLE I. Corrected data summary for angular-distribution measurements. Angles are given in the laboratory system.

E_γ (Mev)	5°	7.5°	10°	12.5°	15°	17.5°	20°
220	76±7	···	80±7	···	70±7	···	82±7
300	92±6	95±7	102±6	91±6	105±6	108±8	94±6
350	74±6	74±6	70±6	68±6	68±6	59±5	62±6
390	57±4	51±5	54±4	58±6	52±3	47±5	46±3

TABLE II. Summary of experimental uncertainties and corrections to the measurement of the energy-dependence of the cross section. Asterisks mark uncertainties less than 1%.

	E_γ 220 Mev	300 Mev	350 Mev	390 Mev
(a) Correction factors for relative energy-dependence measurements				
1. Multiple scattering	1	1.14	1.24	1.37
2. Nuclear scattering and absorption	1	2.2	3.9	9.7
3. Stopper	1	1.04	1.08	1.14
4. Decays in flight	1	0.80	0.75	0.73
5. μ contamination	1	1	0.95	0.85
6. $d\Omega_{c.m.}/d\Omega_{lab}$	1	0.94	0.91	0.86
7. $(p/k)(dk/dp)$	1	0.72	0.68	0.66
8. $kN(k)$	1	1.03	1.03	1.03
Product 1–8	1	1.45	2.3	5.4
(b) Uncertainties affecting relative energy-dependence measurements				
1. Photo energy width due to momentum acceptance of analyzing magnet	±6 Mev	±12 Mev	±14 Mev	±17 Mev
2. Uncertainties affecting intensity:				
Multiple scattering	5%	5%	5%	5%
$\Delta p/p$ acceptance	10%	10%	10%	10%
μ contamination	*	*	5%	10%
Beam monitoring	*	*	2%	2%
Nuclear absorption and scattering	*	*	3%	15%
Subtotal	±12%	±12%	±13%	±22%
3. Possible reduction in correction factor due to revision of nuclear absorption and scattering correction	*	−5%	−12%	−20%

(1) *Absorber corrections.*—The absorber introduces a pion loss due to multiple Coulomb scattering, nuclear absorption and elastic single scattering. These corrections influence the data in two respects: (a) they attenuate the pion beam, and (b) they increase the fraction of muon contamination contributing to the observed counts.

The scattering-out corrections were determined by integrating the theoretical angular distributions of pions scattering in several portions of the absorber over the aperture of the stopper. The angular distributions were (a) the usual Gaussian distribution due to multiple Coulomb scattering, and (b) the diffraction and single Coulomb scattering obtained from an optical model calculation. (These calculations were carried out by the University of California Radiation Laboratory, Livermore, computing group; we are most grateful to Dr. Caris, Dr. Bengston, and Dr. Fernbach for their collaboration.) The optical model caluclations used potentials at each pion energy close to the analysis of Frank, Gammel, and Watson,[9] using values of $r_0=1.14A^{\frac{1}{3}}\times10^{-13}$ cm and $a=0.65\times10^{-13}$ cm in a model in which the nucleon density varies radially as $\{1+\exp[(r-r_0)/a]\}^{-1}$. These calculations were undertaken primarily to fit pion cross-section data taken at 441 Mev by the Berkeley group. Since with the parameters used here the fit of the Berkeley data is not too good, we must consider the scattering-out corrections as preliminary; the uncertainty due to this situation is indicated in the table.

(2) *Other Uncertainties.*—Other uncertainties included in Table II are (a) the uncertainties in the energy dependence of the beam monitoring, referred to above, (b) the uncertainty in the momentum acceptance of the analyzer, and (c) the uncertainty of the μ-contamination corrections.

(3) *Other Corrections.*—Table II also contains a summary of other energy-dependent corrections to the observed counts which can be made without contributing to the probable error of the results such as energy-dependent kinematic factors. One factor labelled "stopper" deserves comment: A separate run showed that the detection efficiency of the counter is a function of the position of the π^+ stopping point within the stopper; since the spatial distribution of π^+ within the stopper is energy-dependent, a small correction factor results. The factor $kN(k)$ represents the number of photons per unit photon energy interval times the photon energy produced per radiation length of radiator per incident electron. This function was computed taking into account the finite radiator thickness and including the effect of self-absorption and a correction to the Bethe-Heitler relation for deviation from Born approximation.

IV. RESULTS

Table I, giving the counts corrected for background, serves directly as a representation of the angular distribution at each energy; they include the small corrections depending on angle. Table III presents the data bearing on the energy dependence. Tabulated are (a) the raw counts including the statistical uncertainty, (b) the correction factor and its uncertainty from Table II, and (c) a final number proportional to the differential cross section; the quoted error includes the systematic uncertainties discussed.

V. INTERPRETATION

We have tried to fit our data to the dispersion-theoretical calculations of Chew *et al.*[5] As mentioned previously, the fit of the available positive-pion photoproduction data from other experiments at larger angles to these calculations is not too satisfactory; hence our ability to reconcile the data reported here with the calculation is of limited significance only.

We state here the complete form of the square of the matrix element used in the calculation, since we find that the information, including all the terms necessary

TABLE III. Relative energy-dependence data (15° lab, 20° c.m.).

E_γ	220 Mev	300 Mev	350 Mev	390 Mev
Uncorrected data (arbitrary normalization)	202±15	116±9	107±7	73±4
Correction factor and uncertainty (from Table II)	1 (12%)	1.45 (12%)	2.3 (13%)	5.4 (22%)
Corrected data	202±28	168±23	246±37	395±90

[9] Frank, Gammel, and Watson, Phys. Rev. **101**, 891 (1956).

for computation, is not now available in a single place.

$$|M|^2=|a|^2+\frac{|b|^2\beta^2(1+\beta^2\gamma^2-2\beta\gamma\cos\theta)(\sin^2\theta\cos^2\varphi)}{(1-\beta\cos\theta)^2}$$
$$+|u|^2\beta^2\gamma^2k^4\sin^2\theta\sin^2\varphi+|v|^2\beta^2\gamma^2k^4\sin^2\theta\cos^2\varphi$$
$$+|w|^2k^4\beta^2\gamma^2\cos^2\theta-\frac{2\,\mathrm{Re}(a^*b)\beta^2\gamma\sin^2\theta\cos^2\varphi}{(1-\beta\cos\theta)}$$
$$-2\,\mathrm{Re}(a^*w)\beta\gamma k^2\cos\theta$$
$$+\frac{2\,\mathrm{Re}(b^*v)k^2\beta^2\gamma\sin^2\theta(1-\beta\gamma\cos\theta)\cos^2\varphi}{(1-\beta\cos\theta)}$$
$$+\frac{2\,\mathrm{Re}(b^*w)\beta^3\gamma^2k^2\cos\theta\sin^2\theta\cos^2\varphi}{(1-\beta\cos\theta)}, \quad (1)$$

where

$$a=-\frac{F_S}{3}(2\delta_1+\delta_3)+i\left(1+\frac{\omega^*}{M}\right)^{-1}\left[1-\frac{\omega^*(g_p-g_n)}{2M}\right], \quad (2)$$

$$b=i\left(1+\frac{\omega^*}{M}\right)^{-1}, \quad (3)$$

$$u=-\frac{2}{9}F_Me^{i\delta_{33}}\sin\delta_{33}-ih^{+-}\left(\frac{g_p-g_n}{4Mf^2}\right), \quad (4)$$

$$v=-\tfrac{1}{3}e^{i\delta_{33}}\sin\delta_{33}(F_Q+\tfrac{1}{3}F_M)$$
$$+i\left[\frac{g_p-g_n}{4Mf^2}h^{--}-\frac{1}{1+(\omega^*/M)}\frac{g_p+g_n}{2M\omega^*}\right], \quad (5)$$

$$w=+\tfrac{1}{3}e^{i\delta_{33}}\sin\delta_{33}(F_Q-\tfrac{1}{3}F_M)$$
$$-i\left[\frac{1}{1+(\omega^*/M)}\frac{g_p+g_n}{2M\omega^*}-\frac{g_p-g_n}{4Mf^2}h^{--}\right]; \quad (6)$$

and the F's are given by[10]

$$F=1+\frac{1-\beta^2}{2\beta}\ln\left(\frac{1-\beta}{1+\beta}\right), \quad (7)$$

$$F_S=1-\tfrac{1}{2}F, \quad (8)$$

$$F_M=\frac{3}{4}\frac{F}{q^2}, \quad (9)$$

$$F_Q=\frac{1}{\omega^{*2}}\left(1-\frac{3}{4\beta^2}F\right); \quad (10)$$

and the h's by

$$h^{--}=\tfrac{1}{3}(h_1-2h_2+h_3), \quad (11)$$

$$h^{+-}=\tfrac{1}{3}(h_1+h_2-2h_3), \quad (12)$$

$$h_1=e^{i\delta_{11}}\sin\delta_{11}/q^3, \quad (13)$$

$$h_2=e^{i\delta_{13}}\sin\delta_{13}/q^3, \quad (14)$$

$$h_3=e^{i\delta_{33}}\sin\delta_{33}/q^2; \quad (15)$$

where $g_p=2.79$ is the proton g factor and $g_n=-1.91$ is the neutron g-factor; $c=1$ is the velocity of light; β is the meson velocity in the c.m. system; γ is the meson total energy (c.m.) divided by the photon energy; θ is the c.m. pion production angle relative to the direction of the photon; φ is the angle between the (q,k) and (k,ϵ) planes, where ϵ is the polarization vector; M is the ratio of the nucleon to the meson rest mass; q is the ratio of the meson c.m. momentum to the meson rest mass; $\omega^*=(q^2+1)^{\frac{1}{2}}+(q^2+M^2)^{\frac{1}{2}}-M$, is the difference between the total energy available in the c.m. system and the nucleon rest mass, divided by the meson rest mass; k is the photon energy in the c.m. system; δ_1 and δ_3 are the s-wave phase shifts; δ_{11}, δ_{33}, and δ_{13} are the p-wave phase shifts with the assumption that $\delta_{13}=\delta_{31}$.

The matrix element is multiplied by

$$2e^2f^2(q/k) \quad (16)$$

to obtain the cross section.

It is assumed that s-wave phase shifts are available from pion-nucleon scattering experiments. We prefer not to use the p-wave phase shifts derived from pion-nucleon scattering experiments since on the one hand the expressions are quite sensitive to the choice of the small p-wave phase shifts (δ_{31}, δ_{13}, δ_{11}), and on the other hand the direct experimental information is poor. Rather, we derive the p-wave phase shifts from the approximate expression of Chew *et al.*[5]:

$$\frac{e^{i\delta_\alpha}\sin\delta_\alpha}{q^3}=\frac{\lambda_\alpha/\omega^*}{1-r_\alpha\omega^*-i(\lambda_\alpha q^3/\omega^*)}, \quad (17)$$

where

$$\lambda_\alpha=\frac{2}{3}f^2\begin{bmatrix}-4\\-1\\+2\end{bmatrix}\quad\text{for}\quad\alpha=\begin{bmatrix}11\\13\\33\end{bmatrix}; \quad (18)$$

and

$$r_{33}=r_{33}{}^0+\frac{9}{8M}=1/\omega_r{}^*, \quad (19)$$

where $\omega_r{}^*$ is the normalized resonance energy; thus permitting evaluation of

$$r_{13}=-\tfrac{4}{5}(r_{33}{}^0), \quad (20)$$

$$r_{11}=-\frac{4}{5}(r_{33}{}^0)-\frac{9}{8M}. \quad (21)$$

[10] The portion of the matrix element arising from the amplitude $\mathfrak{F}^{(0)}$ of Chew *et al.* (reference 5) has been multiplied by the phase space factor $[1+(\omega^*/M)]^{-1}$.

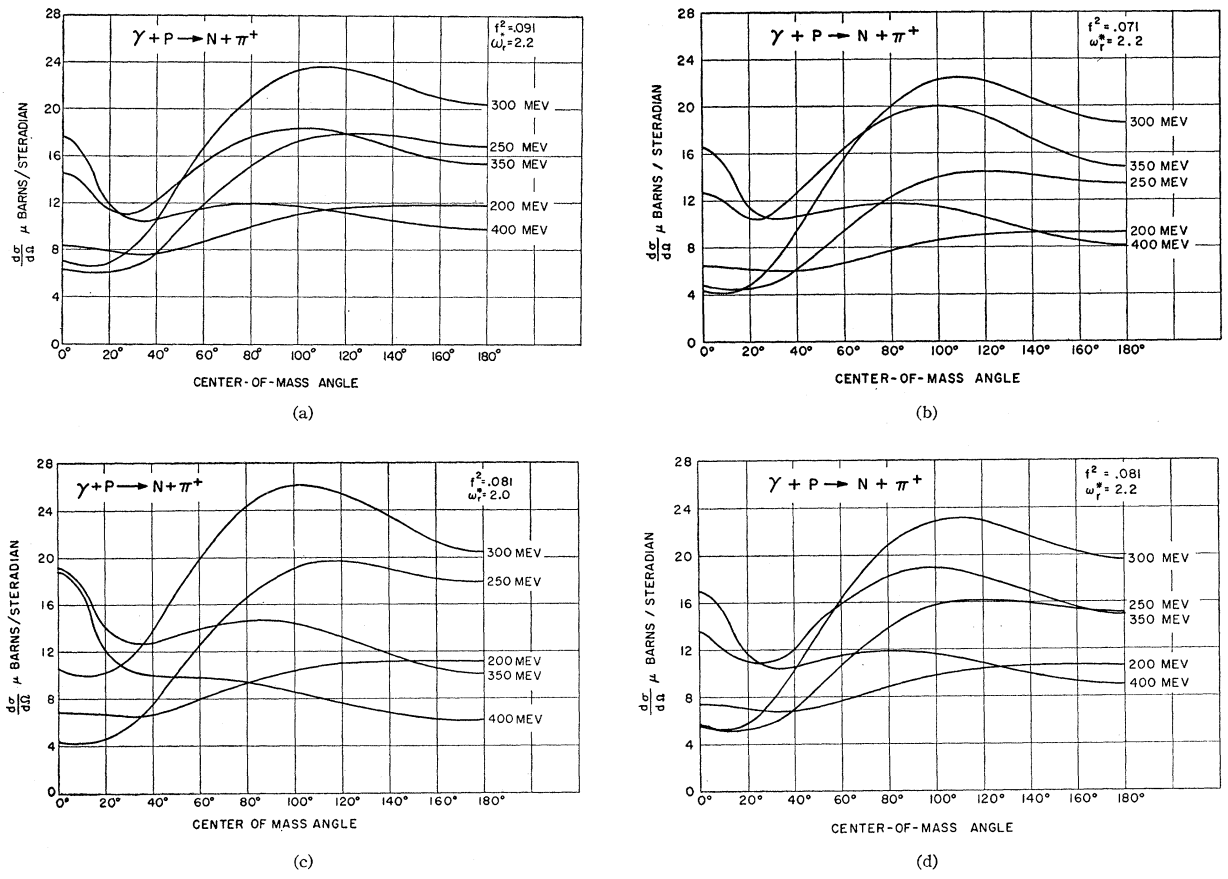

FIG. 7. Plots of the dispersion-theoretical relations of Chew *et al.*[5] giving the cross section for pion photoproduction as a function of c.m. angle. The curves are computed from Eqs. (1)–(21) using the parameters shown in the respective figures.

In the computations we treat f^2 and ω_r^* as free parameters although they are in fact connected by an integral over the total p-wave scattering cross section; within the range of values assumed for f^2 and ω_r^* and the experimental uncertainties of the cross section, this freedom is justified.

In the computation we have used the s-wave phase shifts $\delta_1=0.173q$ and $\delta_3=-0.110q$ as proposed by Puppi[11] to represent the best fit to current pion-nucleon scattering data. We have examined the dependence of the cross sections on the s-wave phase shifts and have found that a 50% change in the s-wave phase shifts produces a 10% change in the cross section for $k=400$ Mev and a 5% change for $k=300$ Mev at the extreme angles $\theta=0$ and $\theta=180°$; at other angles the sensitivity is substantially less.

Equation (1) has been evaluated numerically for the nine cases $f^2=0.071$, 0.081, 0.091, and $\omega_r^*=2.0$, 2.1, and 2.2. Figures 7(a) and (b) show the sensitivity to the choice of renormalized coupling constant f^2, while Figs. 7(c) and (d) show the sensitivity to the choice of the resonance energy ω_r^*.

Figure 8 compares the data of Walker *et al.*[12] and Uretsky *et al.*[13] at large pion angles with the calculations. The figure indicates the present disagreement, which consists primarily of the theoretical resonance cross section being above the experimental points at large production angles.

Our new data at small angles are shown in Fig. 9 in their relation to the angular dependence of the theoretical cross sections; in this figure the absolute values of the measurements have been normalized *at each energy* to the computed curves. (The fit of the energy dependence data is discussed below.) Evidently the agreement is satisfactory.

We have examined the question of the presence of the retardation term by representing both the theoretical and the experimental data by the optimum straight-line fit in the angular interval covered. The results are shown in Table IV. Note that agreement is

[11] G. Puppi, *1958 Annual International Conference on High-Energy Physics at CERN*, edited by B. Ferretti (CERN, Geneva, 1958).

[12] Walker, Teasdale, Peterson, and Vette, Phys. Rev. **99**, 210 (1955).

[13] Uretsky, Kenney, Knapp, and Perez-Mendez, Phys. Rev. Letters **1**, 12 (1958).

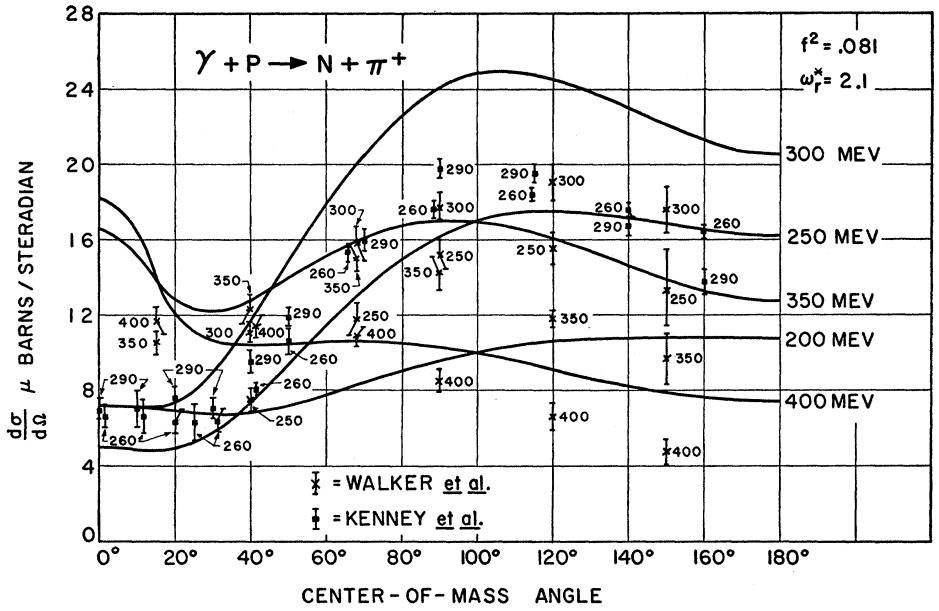

FIG. 8. Plot of the dispersion-theoretical relations for $f^2=0.081$ and $\omega_r^*=2.1$ in comparison with the data of Walker *et al.* (see reference 12) and Uretsky *et al.* (see reference 13).

fair. With the retardation term omitted, the predicted slope would have been positive, in definite contradiction to the data.

It has been generally overlooked that fair evidence for the retardation term exists from the earlier large-angle data.[12] Figure 1 shows the experimental points compared with theory both with and without the retardation term; agreement with the retardation term included is substantially better.

The energy dependence at a fixed c.m. angle of 20° of our small-angle data and those of other workers is compared with these calculations in Fig. 10. Our data are normalized to give the best mean fit to the earlier work, since the measurements are not absolute. The data appear to favor the larger value of the coupling constant; however, this conclusion is fairly weak in view of the general lack of quantitative agreement of the earlier large-angle data[12,13] with the dispersion-theoretical calculations.

VI. ACKNOWLEDGMENTS

The execution of this experiment and its interpretation were aided very substantially by many members of this laboratory and of other organizations. In particular, we acknowledge a number of specific contributions: E. A. Allton constructed the liquid hydrogen target and maintained it during these measurements; Dr. H. C. DeStaebler contributed to the analysis of muon contamination; C. W. Olson and L. Buss took a major part in the design and construction of the electronic apparatus; assistance during the runs was rendered by E. A. Allton, R. A. Alvarez, L. Becker, H. C. DeStaebler, J. Pine, and B. Richter. A. Pittenger helped program the calculations and ran them on the computer.

We are greatly indebted to Dr. S. Fernbach and Dr. J. Bengston of the University of California Radiation Laboratory, Livermore, for the optical-model calcula-

TABLE IV. Fit of the variation of the cross section in the small-angle range by the best straight-line fit.

Photon energy (c.m.)	Slope of cross section (percent variation per degree) Theoretical (mean)	Experimental (least-squares)
350 Mev	−1.29	−1.06±0.48
390 Mev	−2.19	−1.25±0.39

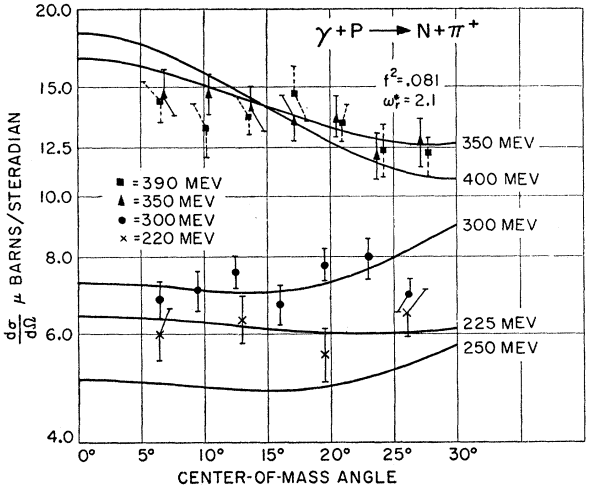

FIG. 9. Plot of the experimental data reported here *vs* c.m. angle, in comparison with the dispersion-theoretical calculations. The data are normalized at each energy.

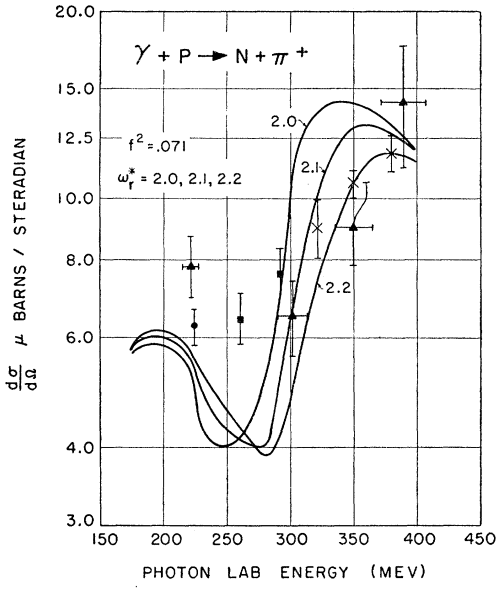

(a)

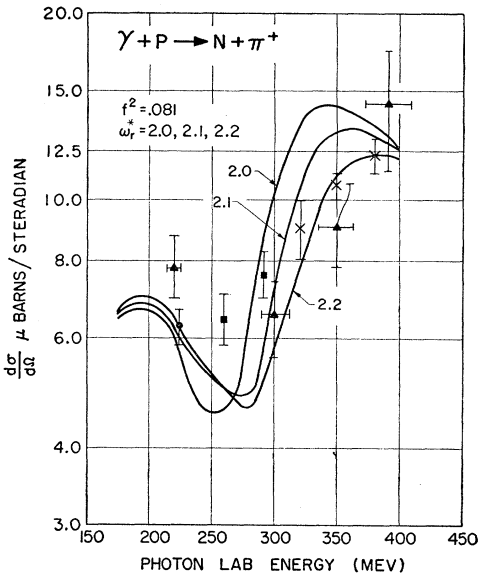

(b)

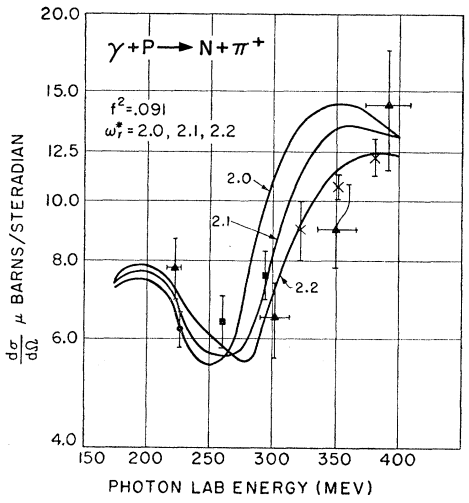

(c)

FIG. 10. Plots of the energy dependence of the cross section at a fixed laboratory angle of 15°. The measurements are the work reported here (triangles), the work of Malmberg and Robinson (reference 4) (circles), Perez-Mendez *et al.* (reference 2) (squares), and Walker *et al.* (reference 12) (crosses). The figures also show the dispersion-theoretical curves with the indicated choice of parameters.

tions on pion scattering in carbon which were used in the scattering-out corrections. We are also indebted to Dr. R. W. Kenney, Dr. V. Perez-Mendez, and Dr. J. C. Caris, University of California Radiation Laboratory, Berkeley, for keeping us informed concerning the progress of their work.

During part of the period of this experiment, one of us (AJL) held a National Science Foundation Fellowship.